










# A Hide-and-seek Game: Looking for Population III Stars during the Epoch of Reionization through the He II $\lambda 1640$ Line

Alessandra Venditti<sup>1,2,3,4</sup> , Volker Bromm<sup>5,6</sup> , Steven L. Finkelstein<sup>5</sup> , Antonello Calabrò<sup>3</sup> , Lorenzo Napolitano<sup>1,3</sup> ,  
Luca Graziani<sup>1,2,3</sup> , and Raffaella Schneider<sup>1,2,3</sup> 

<sup>1</sup> Dipartimento di Fisica, Sapienza, Università di Roma, Piazzale Aldo Moro 5, 00185, Roma, Italy; [alessandra.venditti@inaf.it](mailto:alessandra.venditti@inaf.it)

<sup>2</sup> INFN, Sezione di Roma I, Piazzale Aldo Moro 2, 00185, Roma, Italy

<sup>3</sup> INAF-Osservatorio Astronomico di Roma, Via di Frascati 33, 00078, Monte Porzio Catone, Italy

<sup>4</sup> Dipartimento di Fisica, Tor Vergata, Università di Roma, Via Cracovia 50, 00133, Roma, Italy

<sup>5</sup> Department of Astronomy, University of Texas at Austin, 2515 Speedway, Stop C1400, Austin, TX 78712, USA

<sup>6</sup> Weinberg Institute for Theoretical Physics, University of Texas at Austin, Austin, TX 78712, USA

Received 2024 May 17; revised 2024 August 2; accepted 2024 August 14; published 2024 September 16

## Abstract

The gas surrounding first-generation (Population III, hereafter Pop III) stars is expected to emit a distinct signature in the form of the He II recombination line at 1640 Å (He II  $\lambda 1640$ ). Here we explore the challenges and opportunities in identifying this elusive stellar population via the He II  $\lambda 1640$  in  $M_* > 10^{7.5} M_\odot$  galaxies during the Epoch of Reionization ( $z \simeq 6-10$ ), using JWST/NIRSpec. With this aim in mind, we combine cosmological dustyGadget simulations with analytical modeling of the intrinsic He II emission. While tentative candidates with bright He II emission like GN-z11 have been proposed in the literature, the prevalence of such bright systems remains unclear due to significant uncertainties involved in the prediction of the He II luminosity. In fact, similar Pop III clumps might be almost 2 orders of magnitude fainter, primarily depending on the assumed Pop III formation efficiency and initial mass function in star-forming clouds, while the effect of stellar mass loss is responsible for a factor of order unity. Moreover, up to  $\sim 90\%$  of these clumps might be missed with NIRSpec multi-object spectroscopy due to the limited field of view, while this problem appears to be less severe with NIRSpec's integral field unit. We investigate the potential of deep spectroscopy targeting peripheral Pop III clumps around bright, massive galaxies to achieve a clear detection of the first stars.

*Unified Astronomy Thesaurus concepts:* James Webb Space Telescope (2291); Early universe (435); Galaxy spectroscopy (2171); Population III stars (1285); Reionization (1383); Hydrodynamical simulations (767); High-redshift galaxies (734); Theoretical models (2107)

## 1. Introduction


The deployment of JWST has opened new frontiers for modern astrophysics, enabling us to explore the depth of the high- $z$  Universe with unprecedented sensitivity and resolution. Notably, it paves the way for the exciting possibility of directly detecting the first generation of stars, known as Population III (Pop III) stars.

The He II recombination line at 1640 Å (He II  $\lambda 1640$ ) has been indicated as a potential tracer of Pop IIIs (J. Tumlinson & J. M. Shull 2000; V. Bromm et al. 2001b; J. Tumlinson et al. 2001; D. Schaerer 2002, 2003; A. Raiter et al. 2010). Due to their pristine chemical composition, Pop III stars are expected in fact to be predominantly massive (T. Abel et al. 2002; V. Bromm et al. 2002), up to hundreds of solar masses (T. Hosokawa et al. 2011; S. Hirano et al. 2014; A. Stacy et al. 2016; S. Chon et al. 2024), or even thousands of solar masses (H. Susa et al. 2014; S. Hirano et al. 2015a, 2015b; T. Hosokawa et al. 2016; K. Sugimura et al. 2020; M. A. Latif et al. 2022). This massive component should power a very hard radiation ( $>54.4$  eV), able to doubly ionize helium in the nearby gas, and therefore trigger the He II  $\lambda 1640$  line emission through the cascading recombination of He III.

While Pop III stars are predicted to start forming at Cosmic Dawn, around  $z \sim 20-30$  (V. Bromm 2013; R. S. Klessen & S.

C. O. Glover 2023), cosmological simulations (H. Xu et al. 2016; R. Sarmiento et al. 2018; J. Jaacks et al. 2019; B. Liu & V. Bromm 2020; D. Skinner & J. H. Wise 2020; R. Sarmiento & E. Scannapieco 2022; A. Venditti et al. 2023) and semi-analytical models (E. Visbal et al. 2020; A. Trinca et al. 2024) suggest that pristine gas reservoirs hosting Pop IIIs might persist down to the Epoch of Reionization (EoR;  $z \sim 6-10$ ). There are already a few candidates with tentative He II detection, possibly indicative of Pop IIIs at these epochs (E. Vanzella et al. 2023; R. Maiolino et al. 2024; X. Wang et al. 2024); however, their confirmation is still pending. In fact, similar candidates (e.g., CR7 at  $z \simeq 6.6$ ; D. Sobral et al. 2015) have been rejected in the past on both observational (J. Matthee et al. 2017; R. A. A. Bowler et al. 2017) and theoretical (A. Pallottini et al. 2015; B. Agarwal et al. 2016) grounds, underscoring the importance of using combined diagnostics of spectral hardness and low metallicity to confirm the Pop III nature of these systems (e.g., A. K. Inoue 2011; E. Zackrisson et al. 2011; L. Mas-Ribas et al. 2016; K. Nakajima & R. Maiolino 2022; H. Katz et al. 2023; J. A. A. Trussler et al. 2023; N. J. Cleri et al. 2023).

Despite the plethora of models predicting Pop III star formation at later cosmic times, many observational challenges may account for the lack of clear detections. In fact, Pop III clusters are expected to have low masses (e.g., V. Bromm 2013) and hence be intrinsically faint, so that it might be difficult to detect them even in extremely magnified systems (E. Zackrisson et al. 2012, 2015); their signal may also be further absorbed by interstellar dust (A. Venditti et al. 2023; E. Curtis-Lake et al. 2023; G. Roberts-Borsani et al. 2023).

 Original content from this work may be used under the terms of the [Creative Commons Attribution 4.0 licence](https://creativecommons.org/licenses/by/4.0/). Any further distribution of this work must maintain attribution to the author(s) and the title of the work, journal citation and DOI.

A significant number of Pop III systems at these redshifts might fall outside the field of view (FOV) of our instruments, if they reside at the periphery of their hosting dark matter halos (A. Venditti et al. 2023). Finally, the He II recombination signature is expected to be short-lived, due to the brief lifetime of the most massive stars (a few million years; D. Schaerer 2002, 2003; H. Katz et al. 2023). Understanding all these challenges is crucial in designing robust strategies for a systematic search of Pop IIIs during the EoR, with the goal of expanding our pool of available candidates.

This letter aims to explore all these aspects, by combining the statistics of late Pop III clumps inferred from the cosmological simulations introduced in C. Di Cesare et al. (2023) and A. Venditti et al. (2023) with an analytical modeling of the He II emission arising from Pop III stars (D. Schaerer 2002). In Section 2, we describe our cosmological simulations (Section 2.1) and the adopted procedure to estimate the He II luminosity from Pop III stellar populations (Section 2.2). In Section 3, we present our results, i.e., (i) our predictions of the He II luminosity, compared with the sensitivity of JWST/NIRSpec in different configurations (Section 3.1); (ii) the expected bias due to the limited FOV (Section 3.2); and (iii) the expected number of He II-emitting Pop III systems in existing JWST surveys (Section 3.3). In Section 4, we critically discuss our findings, with particular reference to the effect of dust absorption/scattering (Section 4.1) and to the potential of using He II for the identification of Pop III stars compared to other indicators, e.g., pair-instability supernovae (PISNe; Section 4.2). Finally, Section 5 presents our conclusions.

## 2. Methodology

### 2.1. Simulating the Cosmological Environment

The cosmological simulations employed in the present work have been performed with the hydrodynamical code `dustyGadget` (L. Graziani et al. 2020), and they are described in C. Di Cesare et al. (2023). They consist of eight simulated volumes (U6—U13), with a comoving side of  $50h^{-1}$  cMpc, a total number of  $2 \times 672^3$  particles, and a mass resolution for dark matter/gas particles of  $3.53 \times 10^7 h^{-1} M_\odot / 5.56 \times 10^6 h^{-1} M_\odot$  each, evolved from  $z \simeq 100$  down to  $z \simeq 4$ .<sup>7</sup> A Lambda cold dark matter ( $\Lambda$ CDM) cosmology consistent with Planck Collaboration et al. (2016) is assumed ( $\Omega_{m,0} = 0.3089$ ,  $\Omega_{b,0} = 0.0486$ ,  $\Omega_{\Lambda,0} = 0.6911$ , and  $h = 0.6774$ ).

Detailed information on the `dustyGadget` code, and particularly on its innovative self-consistent modeling for dust production and evolution, can be found in L. Graziani et al. (2020). The code extends the original implementation of the SPH code `Gadget-2` (V. Springel 2005), on top of the improvements to the chemical evolution module from L. Tornatore et al. (2007a, 2007b), to molecular chemistry and cooling from U. Maio et al. (2007) and to their coupling with Pop III/II formation from U. Maio et al. (2010, 2011). We here briefly summarize the main features of the adopted prescriptions for star formation and feedback, of particular interest for the present work.

A two-phase interstellar medium (ISM) model is implemented for each SPH gas particle, following V. Springel & L. Hernquist (2003). Stellar particles with a mass of  $\sim 2 \times 10^6 M_\odot$  are generated from gas particles with a number density ( $n$ ) above the threshold  $n_{\text{th}} \simeq 300 \text{ cm}^{-3}$ ; the cold-gas phase is depleted into stars at a rate  $n_{\text{cold}}/t_*$ , with  $n_{\text{cold}}$  the cold-phase number density and  $t_* = 2.1 \text{ Gyr} \times (n/n_{\text{th}})^{-1/2}$  the characteristic timescale of the process. The stellar particles represent stellar populations born in an instantaneous burst with an assigned initial mass function (IMF). Depending on the gas metallicity, below or above a critical metallicity ( $Z_{\text{crit}} = 10^{-4} Z_\odot$ ; V. Bromm et al. 2001a; U. Maio et al. 2010; L. Graziani et al. 2020) we define a stellar population to be Pop III or Population II/I (Pop II/I), respectively.<sup>8</sup> We assume a Salpeter-shaped IMF (E. E. Salpeter 1955) with a mass range of  $[0.1, 100]$  ( $[100, 500]$ )  $M_\odot$  for Pop II/I (Pop III); this results in an average lifetime for Pop III stars of  $\simeq 3 \text{ Myr}$  (see Equation (1) of A. Venditti et al. 2023). The impact of the contribution of low-mass Pop III stars, ( $\sim 1\text{--}40 M_\odot$ , the mass range inferred from stellar archeology; N. Iwamoto et al. 2005; M. de Bennassuti et al. 2014; M. N. Ishigaki et al. 2014; S. C. Keller et al. 2014; T. Hartwig et al. 2015; M. de Bennassuti et al. 2017; M. Fraser et al. 2017; M. Rossi et al. 2021; M. Magg et al. 2022; D. S. Aguado et al. 2023) is extensively discussed in A. Venditti et al. (2023, 2024). In fact, although the aforementioned studies show that a precise modeling of the low-mass end of the IMF is required to reconstruct the detailed nucleosynthetic pattern of old, metal-poor stars, here we are mostly interested in the high-mass tail that is mainly responsible for He ionization, because of its hard UV photon budget. However, it is important to emphasize that changing the IMF in a way that influences the power at high masses—either via changes in its shape or mass range—can affect our results (see the discussion in Section 2.2).

The gas chemical evolution model is adopted from L. Tornatore et al. (2007a) and U. Maio et al. (2010, 2011). We include mass-dependent yields from Pop III stars in the range  $[140, 260] M_\odot$ , ending their life as PISNe (A. Heger & S. E. Woosley 2002), and mass- and metallicity-dependent yields from Pop II/I stars with low-to-intermediate mass (long-lived; L. B. van den Hoek & M. A. T. Groenewegen 1997) and high-mass ( $> 8 M_\odot$ , dying as core-collapse supernovae; S. E. Woosley & T. A. Weaver 1995), also considering Type Ia supernovae (F. K. Thielemann et al. 2003). For simplicity, we assume that Pop II/I stars more massive than  $40 M_\odot$  and Pop III stars outside the PISN range directly collapse into black holes and do not participate in the metal-enrichment process. This clearly is an idealization, and effects such as rapid rotation could contribute to enrichment across a broader range of stellar masses (e.g., B. Liu et al. 2021). Dust and metals are spread in the ISM through a spline kernel. Galactic winds are also modeled following V. Springel & L. Hernquist (2003), with a constant velocity of  $500 \text{ km s}^{-1}$  (L. Tornatore et al. 2010; U. Maio et al. 2011).

The simulations have demonstrated good agreement with available model predictions and observations of the cosmic star formation rate/stellar mass density evolution and with important scaling relations (i.e., the main sequence of star-forming galaxies, the stellar-to-halo mass relation, and the dust-to-stellar mass relation), including early JWST data (C. Di Cesare et al. 2023); we emphasize here that our model is not calibrated on

<sup>7</sup> Data from U9 and U11 are not included in the present work as these simulations present different snapshot dumpings with respect to the others; in fact, these cubes are less star-forming and hence of lower interest for the present study.

<sup>8</sup> Here we assume  $Z_\odot = 0.02$  (E. Anders & N. Grevesse 1989).

any particular observational set or survey. The simulations have also been employed to investigate carbon envelopes around merging galaxies as a possible origin of the [C II]158  $\mu\text{m}$  emission in the circumgalactic medium surrounding individual, resolved galaxies, observed by the ALPINE survey at  $z \sim 4.5$  (C. Di Cesare et al. 2024).<sup>9</sup> Most notably, they are the largest simulated volumes currently available that include a model for Pop III stars, making them a powerful tool to understand the statistics of Pop III star formation across cosmic time (A. Venditti et al. 2023, 2024). However, we emphasize that the limited mass resolution, together with the lack of a proper treatment of radiative feedback,<sup>10</sup> allows us to provide reliable results only for halos with a stellar mass of  $\log(M_*/M_\odot) \gtrsim 7.5$  at  $6 \lesssim z \lesssim 10$ ;<sup>11</sup> note that all Pop III stars in this mass regime at the considered redshifts are found to be coexisting with Pop II stellar components in our simulations (A. Venditti et al. 2023). We also currently do not include a model for metal mixing and turbulent metal diffusion below our gas mass resolution as, for example, in R. J. Sarmiento et al. (2016), R. Sarmiento et al. (2017, 2018), and R. Sarmiento & E. Scannapieco (2022). We refer the reader to A. Venditti et al. (2023, 2024) for a thorough discussion of these limitations for Pop III studies.

## 2.2. Computing the He II Luminosity of Pop III Clumps

The intrinsic luminosity of the He II  $\lambda 1640$  line ( $L_{\text{HeII}}$ ) emitted from a Pop III clump (i.e., a Pop III stellar cluster, represented by a stellar particle in our simulations as defined in Section 2.1) can be inferred from the mass of the clump ( $M_{\text{III}}$ ) as follows:

$$L_{\text{HeII}} = \bar{\epsilon}_{\text{HeII}} E_{\text{HeII}} \times M_{\text{III}}, \quad (1)$$

with  $E_{\text{HeII}} \simeq 1.21 \times 10^{-11}$  erg the energy of a He II  $\lambda 1640$  photon and  $\bar{\epsilon}_{\text{HeII}}$  the average He II photon emissivity per unit stellar mass of a Pop III stellar population. We do not take into account dust attenuation, the expected impact of which will be further discussed in Section 4.1.

Figure 1 shows the time-averaged photon production rate  $\epsilon_{\text{HeII}}$  of individual Pop III stars of various masses  $m$  (averaged over the lifetime of each star), assuming either strong mass loss (Strong ML, dotted line) or no mass loss at all (No ML, solid line), from Tables 5 and 4 of D. Schaerer (2002), respectively. We compute  $\bar{\epsilon}_{\text{HeII}}$  by integrating over the IMF  $\phi(m)$ :

$$\bar{\epsilon}_{\text{HeII}} = \frac{\int_{m_{\text{low}}}^{m_{\text{up}}} \epsilon_{\text{HeII}}(m) \phi(m) dm}{\int_{m_{\text{low}}}^{m_{\text{up}}} \phi(m) dm}. \quad (2)$$

For our assumed Salpeter-like IMF (whose lower and upper limits are  $m_{\text{low}} = 100 M_\odot$  and  $m_{\text{up}} = 500 M_\odot$ ; Section 2.1), this results in  $\bar{\epsilon}_{\text{HeII}} \simeq 1.53 \times 10^{47} / 6.48 \times 10^{46}$  phot.  $\text{s}^{-1} M_\odot^{-1}$  for the cases with strong/no mass loss, respectively. By considering a wide range of possible IMFs (as in Table 1 of A. Venditti et al.

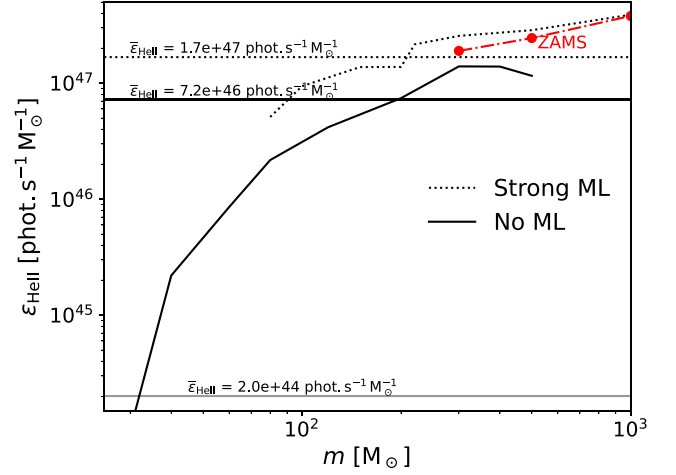


**Figure 1.** Time-averaged He II photon emissivity per unit stellar mass  $\epsilon_{\text{HeII}}$  as a function of the initial Pop III mass  $m$ , from D. Schaerer (2002). The black solid line refers to the model assuming no mass loss (no ML; see Table 4 of the original paper), while the black dotted line refers to the model assuming strong mass loss (strong ML; see their Table 5). The average emissivity  $\bar{\epsilon}_{\text{HeII}}$  of Pop III stellar populations for the two models with our assumed Salpeter-like IMF in the range  $[100, 500] M_\odot$ , i.e., the values adopted in Equation (2) for the present work, are indicated on top of the horizontal solid/dotted black lines; the value for a Salpeter-like IMF in the range  $[1, 1000] M_\odot$  with no ML is also indicated on top of the horizontal solid gray line (see text for details). The red dashed-dotted line further shows the cases of  $300 M_\odot$ ,  $500 M_\odot$ , and  $1000 M_\odot$  stars evolving on the ZAMS along the entire stellar lifetime as a reference (V. Bromm et al. 2001b), to exemplify how mass loss keeps stellar evolution closer to the ZAMS, enhancing the time-averaged photon emissivity (as in the black dotted line).

2024), we find that this value can become up to  $\sim 350$  times lower depending on the adopted IMF (in particular, this value is found for a Salpeter-like IMF in the range  $[1, 1000] M_\odot$ , with no mass loss).<sup>12</sup> Note that mass loss causes the stars to evolve close to the zero-age main sequence (ZAMS) for longer times, resulting in higher time-averaged photon emissivities.<sup>13</sup> In fact, the model of V. Bromm et al. (2001b)—assuming Pop III stars always evolving along the ZAMS—lies closer to the strong-mass-loss case (red dashed-dotted line).<sup>14</sup>

As in A. Venditti et al. (2024), we consider the possibility of a Pop III mass,  $M_{\text{III}}$ , in our Pop III clumps (in Equation (1)) that is lower than our resolution element  $M_{\text{III,res}} \sim 2 \times 10^6 M_\odot$  (i.e., the mass of a Pop III stellar particle in our simulations), by introducing an efficiency factor  $\eta_{\text{III}} < 1$ :

$$M_{\text{III}} = \eta_{\text{III}} M_{\text{III,res}}. \quad (3)$$

<sup>12</sup> As D. Schaerer (2002) does not provide results for the He II emissivity below a mass of  $8/5 M_\odot$  (for the cases with strong/no mass loss, respectively), we conservatively assume that the time-averaged emissivity in Equation (2) is zero below the available mass range. This is a good approximation for the no-mass-loss case as the He II emissivity has dropped by more than 12 orders of magnitude between the example of a  $500 M_\odot$  and  $5 M_\odot$  star (see Table 4 of D. Schaerer 2002). We further assume that the He II emissivity for a  $1000 M_\odot$  star in the no-mass-loss case—also not provided in D. Schaerer (2002)—is the same with respect to a  $500 M_\odot$  star; in fact, the production rates per unit mass of stars  $> 300 M_\odot$  are found to be essentially independent of stellar mass, within a factor 2 (V. Bromm et al. 2001b).

<sup>13</sup> We emphasize that the emission model for Pop III stars is not consistent with the feedback model of the simulations. Similar to A. Venditti et al. (2024), in fact, we only explore how our assumptions on Pop IIIs affect the He II emissivity in post-processing, while a complete discussion would require a self-consistent treatment, also taking into account their impact on the overall star formation history.

<sup>14</sup> Shown for the cases of  $300 M_\odot$ ,  $500 M_\odot$ , and  $1000 M_\odot$  Pop III stars. See Table 1 of V. Bromm et al. (2001b) for the case of a  $1000 M_\odot$  Pop III star; the  $300 M_\odot$  and  $500 M_\odot$  values are obtained from private communication.

<sup>9</sup> ALMA Large Program to Investigate [C II] at Early Times Survey (A. L. Faisst et al. 2020; M. Béthermin et al. 2020; O. Le Fèvre et al. 2020) <http://alpine.ipac.caltech.edu/>.

<sup>10</sup> The simulations only include a homogeneous UV background as in F. Haardt & P. Madau (1996) at  $z < 6$ , hence neglecting the effect of radiative feedback on cosmic star formation at higher redshifts. See Appendix A of A. Venditti et al. (2023) for a discussion of the impact of neglecting UV and Lyman–Werner feedback on the overall Pop III star formation history, in the considered redshift range and at the considered resolution.

<sup>11</sup> Corresponding to a number of stellar particles  $\gtrsim 20$ .

By interpreting  $M_{\text{III, res}}$  as the amount of extremely metal-poor gas above our density threshold that is available for star formation, and  $M_{\text{III}}$  as the amount of stellar mass actually produced in a single star formation event, we can place a lower limit on  $\eta_{\text{III}} \sim 0.01$  from simulations describing Pop III star formation in the first minihalos (see, e.g., V. Bromm 2013, and references therein).<sup>15</sup> However, higher values might be found in more massive halos at later times, which are expected to host more efficient star formation sites. In fact, a past simulation (T. H. Greif et al. 2008) of primordial gas collapsing into an atomic cooling halo at  $z \sim 10$  shows that the gas experiences a boost in ionization (e.g., through shocks), resulting in more efficient cooling through the HD channel (V. Bromm et al. 2009); this intermediate regime—previously referred to as Pop III.2 or Pop II.5—between the very first episodes of star formation and later Pop II/I star formation has been predicted to yield higher star formation efficiencies, even a factor  $\sim 10$  higher than star formation in minihalos at Cosmic Dawn (T. H. Greif & V. Bromm 2006). In the absence of tight constraints in the mass regime we are currently probing, we explore values up to  $\eta_{\text{III}} \sim 0.1$ . We note that a similar value would also be implied considering the ratio of the mass inferred for the supposed Pop III clusters in GN-z11 at  $z = 10.6$  ( $\sim 2\text{--}2.5 \times 10^5 M_{\odot}$ ; R. Maiolino et al. 2024) and RXJ2129-z8HeII at  $z \simeq 8.2$  ( $7.8 \pm 1.4 \times 10^5 M_{\odot}$ ; X. Wang et al. 2024) with respect to our resolution element.<sup>16</sup>

Using the He II line alone to distinguish between the underlying emission model for Pop III stars is challenging, due to the degeneracy among all the uncertain parameters that determine the He II luminosity. However, in Section 3.1, we provide a broad range of possible values for  $L_{\text{HeII}}$  to offer clues on the sensitivity required to rule out the presence of Pop III stars in high- $z$  galaxies, taking into account the considerable uncertainties on their nature.

### 3. Results

#### 3.1. He II Luminosity versus JWST/NIRSpec Sensitivity

Figure 2 provides predictions of the He II luminosity ( $L_{\text{HeII}}$ ) arising from *dustyGadget* galaxies hosting Pop IIIs as a function of redshift  $z$ , considering different assumptions on the Pop III formation efficiency  $\eta_{\text{III}}$  and mass loss. We estimate the average Pop III mass ( $M_{\text{III}} \simeq 2.24 \times 10^6 M_{\odot}$ ) in Pop III-hosting galaxies above  $M_{\star} \simeq 10^{7.5} M_{\odot}$  between redshifts  $\sim 6$  and  $\sim 10$ , and compute the resulting  $L_{\text{HeII}}$  from Equation (1). The upper end of the shaded regions in the plots is associated with the models assuming strong mass loss and high  $\eta_{\text{III}}$  (up to a value  $\eta_{\text{III}} = 0.3$ ), while the lower end is associated with no mass loss and low  $\eta_{\text{III}}$  (down to  $\eta_{\text{III}} = 0.01$ ).<sup>17</sup> The  $L_{\text{HeII}}$  spread is dominated by the uncertainty on  $\eta_{\text{III}}$ , while the presence/absence of mass loss only accounts for a factor of order unity. As discussed in Section 2.2, considering a different IMF can lead to lower

luminosities, up to a factor  $\sim 1/350$ ; moreover, these results do not account for dust absorption, which might lead to very high attenuations (up to a factor  $\sim 10^{-9}$ ) along particularly unfavorable lines of sight, although along more typical lines of sight less than 10% of the flux would be absorbed (see the discussion in Section 4.1). The purple, green, and blue stars provide a comparison with the luminosity of available observational candidates, i.e., LAP1 at  $z \simeq 6.6$  (E. Vanzella et al. 2023),<sup>18</sup> RXJ2129-z8HeII at  $z \simeq 8.2$  (X. Wang et al. 2024), and GN-z11 at  $z \simeq 10.6$  (R. Maiolino et al. 2024).<sup>19</sup>

The oblique lines indicate sensitivity limits for JWST/NIRSpec (P. Jakobsen et al. 2022) in both the integral field unit (IFU) and multi-object spectroscopy (MOS) modes at  $z \simeq 6.7$  and  $z \simeq 10$  for different configurations. The limits are computed using version 4.0 of the JWST Exposure Time Calculator,<sup>20</sup> assuming a point source with no continuum,<sup>21</sup> and a line centered at  $\lambda \simeq 1.64 \times [(1+z)/10] \mu\text{m}$ , plus medium background.<sup>22</sup> We adopt an operational integrated signal-to-noise ratio (S/N) threshold of  $\sim 3$  to determine the minimum observable line flux, which depends on the specific observational setup as well as the chosen line width. We explore two possible values for the line width,  $\Delta v = 500/50 \text{ km s}^{-1}$  (dashed-dotted lines), corresponding respectively to typical virial velocities in high- $z$  galaxies ( $\Delta v \simeq 50 \text{ km s}^{-1}$ ), and to a more extreme scenario, typical of feedback-generated velocities, such as supernova-driven outflows ( $\Delta v \simeq 500 \text{ km s}^{-1}$ ).<sup>23</sup> We further consider observations with two exposure times,  $t \simeq 10/50 \text{ hr}$  (gray/golden lines), with the appropriate grating/filter pair depending on the redshifted wavelength of the line at medium/high resolution (i.e., resolving power  $R = 1000/2700$ ) and with the Prism/CLEAR at low resolution ( $R = 100$ ).<sup>24</sup>

<sup>18</sup> Note that, while the authors provide constraints on the expected He II flux in LAP1, the identification of the observed feature as a He II  $\lambda 1640$  line is weakened by the presence of a small blueshift relative to the Balmer lines. Moreover, the measured flux would require a quite extreme Pop III scenario. Hence, the authors conservatively consider the line nondetected and derive an upper limit on the He II flux, also shown in the plot.

<sup>19</sup> The two points for GN-z11 in the left panel indicate two different NIRSpec/IFU measures, considering a small aperture around the He II clump (bottom point) and a larger aperture aimed at also capturing an additional, more extended emission, possibly coming from a fainter, less significant clump (top point). The point in the right panel refers instead to the NIRSpec/MOS measure. Although the two measures are consistent in terms of wavelength, comparing the fluxes is nontrivial due to the uncertainty on the exact location of the MSA shutter, and hence on the covered fraction of the putative He II clump (R. Maiolino et al. 2024).

<sup>20</sup> <https://jwst.etc.stsci.edu>

<sup>21</sup> If the continuum is detected, this will effectively boost the line. For example, by considering a flat continuum of  $\sim 1\text{--}10 \text{ nJy}$ , the total S/N at the wavelength of the line is approximately enhanced by a quantity of the order of the S/N for the detection of the continuum itself.

<sup>22</sup> Backgrounds in the ETC are obtained using a background model generator accounting for the various components that contribute to the JWST background (J. R. Rigby et al. 2023). In particular, a medium background accounts for the 50% percentile over the period of visibility in a given celestial position. We used as a reference the position of the He II clump in GN-z11, for consistency among the various calculations. By considering, for example, the position of LAP1 and RXJ2129-z8HeII, we find a variation up to  $\sim 8\%$  (specifically, for the position of RXJ2129-z8HeII) in the expected S/N at the same limiting flux.

<sup>23</sup> A similar value of  $\Delta v \simeq 428 \text{ km s}^{-1}$  has been found for the He II  $\lambda 1640$  line detected in the lensed galaxy RXCJ2248-ID at  $z = 6.1$  (M. W. Topping et al. 2024), whose spectrum broadly resembles that of GN-z11 (R. Maiolino et al. 2024), minus the active galactic nuclei signatures.

<sup>24</sup> For the PRISM/CLEAR, only the  $500 \text{ km s}^{-1}$  case is shown, as the instrument cannot discriminate emission lines with  $\Delta v \lesssim 5000 \text{ km s}^{-1}$  at these wavelengths, and hence using a lower  $\Delta v$  does not change the results.

<sup>15</sup> We note that, although in the present study we focus on Pop III stellar clusters, the formation of isolated Population III stars with masses between  $\sim 100$  and  $500 M_{\odot}$  has also been considered in the literature (e.g., H. Katz et al. 2023), and previous studies (e.g., C.-E. Rydberg et al. 2013; R. A. Windhorst et al. 2018) seem to indicate that such individual Population III stars would be too faint to be observed unless subject to extreme gravitational lensing.

<sup>16</sup> The mass estimate from R. Maiolino et al. (2024) has been updated with respect to A. Venditti et al. (2024) to match the accepted version of the paper.

<sup>17</sup> This upper limit is derived by considering the ratio of the Pop III mass inferred for RXJ2129-z8HeII ( $\sim 7.8 \times 10^5 M_{\odot}$ ) to our typical Pop III stellar particle masses.

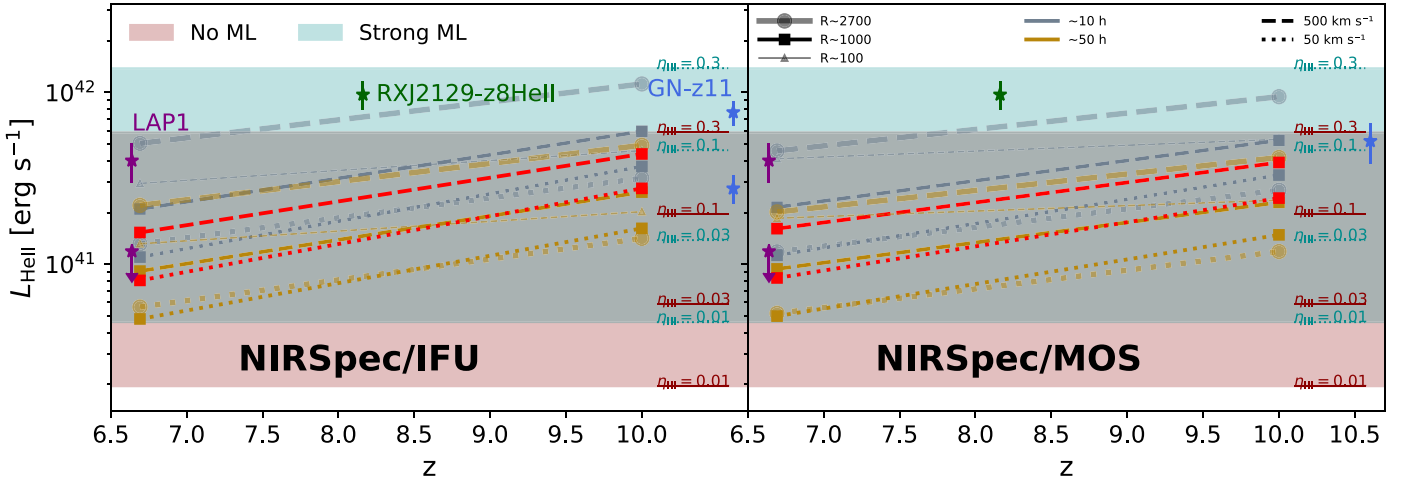


**Figure 2.** Average He II line luminosity ( $L_{\text{HeII}}$ , shaded regions) arising from Pop III-hosting dustyGadget galaxies at  $z \sim 6.7$ –10, assuming a Salpeter-like IMF in the range  $[100, 500] M_{\odot}$ , compared with available observational candidates, i.e., LAP1 at  $z \simeq 6.6$  (E. Vanzella et al. 2023, purple stars), RXJ2129-z8HeII at  $z \simeq 8.2$  (X. Wang et al. 2024, green star), and GN-z11 at  $z \simeq 10.6$  (R. Maiolino et al. 2024, blue stars). The dark red/dark cyan shaded regions refer to the models assuming no/strong mass loss (No ML/Strong ML), respectively, with variable Pop III formation efficiency  $\eta_{\text{III}}$  from 0.01 (lower end of the regions) to 0.3 (upper end), and considering the average Pop III mass in dustyGadget galaxies at these redshifts in Equation (1). The oblique lines show the sensitivity of JWST/NIRSpect corresponding to an integrated S/N  $\sim 3$  line detection in both the IFU (left) and MOS (right) observing modes at  $z \simeq 6.7$  and  $z \simeq 10$  for different configurations, i.e., different resolving powers ( $R \sim 1000/2700/100$ , with different thickness and markers), exposure times ( $\sim 10/50$  hr; gray/golden), and line widths ( $500/50 \text{ km s}^{-1}$ ; dashed-dotted). The corresponding lines for an integrated S/N  $\sim 5$  line detection with medium resolving power and a  $\sim 50$  hr exposure are also shown in red, with the same line styles as the S/N  $\sim 3$  case for the two assumed line widths.

In the IFU mode, the instrument is centered on the source with an aperture<sup>25</sup> of  $0''.09$ , while the sky annulus<sup>26</sup> spans a range between  $0''.3$  and  $0''.9$ . In the MOS mode, we select a three-shutter ( $-1, 0, 1$ ) slitlet shape, with the source placed in shutter 0 and the micro-shutter assembly (MSA) located in quadrant 3 center; we apply the MSA full shutter extraction strategy for background subtraction. The improved reference sampling and subtraction (IRS<sup>2</sup>; B. J. Rauscher et al. 2012) readout pattern is employed for both cases.

It is evident that even with  $\sim 10$  hr observations and considering the narrow-line, best-case scenario at all the available spectral resolutions, we would only be able to capture very luminous Pop III systems ( $L_{\text{HeII}} \gtrsim 10^{41} \text{ erg s}^{-1}$ , i.e., assuming  $\eta_{\text{III}} \gtrsim 0.02/0.06$  in the strong/no-mass-loss cases). All the observed candidates lie in fact in the upper part of this plot. Very-low-luminosity systems ( $\lesssim 4 \times 10^{40} \text{ erg s}^{-1}$ ) would be missed even in the deepest exposures ( $\sim 50$  hr). However, it is to be noted that more favorable conditions are possible. For example, while here we conservatively assumed a medium background, the very low background during the NIRSpect/IFU observation of GN-z11 allowed the detection of a fainter He II line than expected (with a  $\simeq 10.6$  hr exposure, in the small aperture). Moreover, the line appears unresolved in the G235M/F170LP grating/filter pair ( $R \sim 1000$ ), meaning even narrower lines (with higher S/N) may be found.

### 3.2. Pop IIIs outside JWST/NIRSpect’s Field of View

Another factor contributing to the potential oversight of Pop III systems is their placement outside the FOV of our instruments. As star formation is typically more efficient in the dense, central regions of galaxies (e.g., E. R. Carrasco et al. 2010; P. G. van

Dokkum et al. 2014), peripheral areas tend to evolve at a slower pace, preserving their chemically pristine state for extended periods of time; additionally, these regions may experience gas infall from the external environment. Pristine star-forming regions may also reside in small satellites at the periphery of the same dark matter halo. As a result, Pop III stars might be found as far as  $\sim 20$  kpc from the galactic center (see Figure 10 of A. Venditti et al. 2023), especially in regions surrounding massive, evolved galaxies, which have undergone prolonged periods of star formation. For example, R. Maiolino et al. (2024) find a potential Pop III clump at a distance  $\sim 2$  kpc from the host galaxy of GN-z11 ( $M_{\star} \sim 8 \times 10^8 M_{\odot}$ ).

We estimate the number of Pop III systems that might be missed in a single pointing of JWST/NIRSpect centered on dustyGadget halos. Note that 2 degrees of freedom need to be taken into account in this calculation:

1. The orientation of the galaxy with respect to our instruments. In fact, when projecting a three-dimensional galaxy onto a two-dimensional image on the sky along an arbitrary direction, the hosted Pop III cluster will be observed at a distance  $d_{\text{proj}}$  from the galactic center which is at most equal to the three-dimensional distance  $d_{3\text{D}}$ . In particular, there is always a direction along which the Pop III cluster is exactly aligned with the center along our line of sight to the source. For each simulated galaxy, we consider the worst possible projection in which  $d_{\text{proj}} = d_{3\text{D}}$ , hence providing an upper limit on the number of Pop III systems that we expect to be missing when pointing toward the galactic center. We further consider the case of an average line of sight ( $\langle d_{\text{proj}} \rangle = d_{3\text{D}} \times \pi/4$ ).
2. The orientation of the instrument. As shown in Figure 3, we consider two cases: (i) a Pop III system is “missed” when we are never able to see it however we rotate the FOV, i.e., when  $d_{\text{proj}} > d_{\text{max}}$  (falling out of the solid circumferences encompassing all the possible orientations of the instrument); (ii) a Pop III system is “potentially missed” when it might be missed depending on the

<sup>25</sup> As we aim for the smallest possible aperture in order to optimize the sampled flux at the center, we consider a value of the order of the point-spread function FWHM at  $\lambda \sim 1.5 \mu\text{m}$  (as a reference, note that the line is redshifted at  $\lambda \simeq 1.3/1.8 \mu\text{m}$  at  $z \simeq 6.7/10$ , respectively).

<sup>26</sup> The choice of the sky annulus used for background subtraction does not change our results appreciably, as we are considering a uniform background.

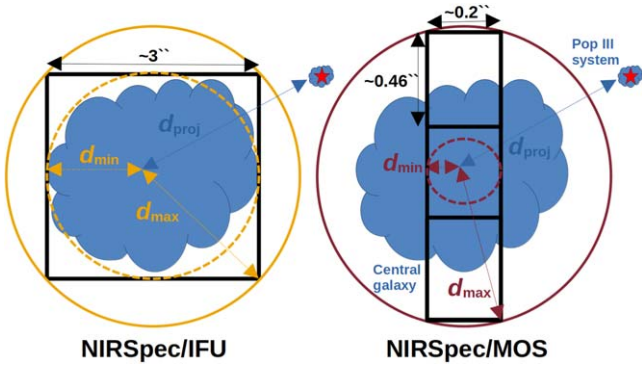


**Figure 3.** Illustration of a single JWST/NIRSpec pointing centered on Pop III-hosting galaxies (blue clouds) in the IFU/MOS modes, respectively (left/right; in the MOS mode, three consecutive shutters are considered). The distances  $d_{\text{proj}}$  of the peripheral Pop III clusters (small blue clouds and red stars) from the galactic center in the displayed projection are shown as blue arrows, while the largest distances such that the clusters would certainly fall within the FOV independent of the instrument’s orientation ( $d_{\text{min}}$ ), or that conversely they would fall within for at least one possible orientation ( $d_{\text{max}}$ ), are shown as dashed–solid arrows, spanning the whole dashed–solid circumferences. The dimensions of the NIRSpec/IFU FOV and of the three shutters of NIRSpec/MOS are also indicated in the figure (not to scale). Depending on the orientation of the galaxies with respect to our instruments, peripheral Pop III systems might fall out of the FOV and would thus be missed in observations.

particular orientation of the FOV, i.e.,  $d_{\text{proj}} > d_{\text{min}}$  (falling out of the dashed circumference enclosing the area always covered with a random, fixed orientation of the instrument). For the IFU/MOS NIRSpec modes (the latter assumed in a three-shutter configuration), we have  $d_{\text{max}} \simeq 2'' 1/1'' 0$  and  $d_{\text{min}} \simeq 1'' 5/0'' 1$ .

The top panels of Figure 4 show the number density of Pop III particles that would be found within the NIRSpec FOV in all the considered configurations, compared to the total; we remark that the average lifetime of Pop III stars with our assumed IMF is  $\simeq 3$  Myr (see Section 2.1), which is consistent with predictions for the lifetime of He II signatures found by previous works (e.g., D. Schaerer 2002, 2003; H. Katz et al. 2023). Results are shown at  $z = 8.1, 7.3$ , and  $6.7$  in bins<sup>27</sup> of stellar mass  $M_*$ .<sup>28</sup> The bottom panels illustrate, conversely, the fraction of Pop IIIs missed in all the aforementioned scenarios. We find that a significant number of Pop III systems can be overlooked in these configurations, especially in high-mass galaxies, although this problem appears to be less severe with NIRSpec/IFU thanks to its larger FOV.

Note that, in the case of GN-z11, the He II  $\lambda 1640$  emission found to peak at about  $d_{\text{proj}} = 0''.5$  from the center (i.e.,  $d_{\text{min}} < d_{\text{proj}} < d_{\text{max}}$  for the MOS mode) would have been missed with a different orientation of the MSA, while it is always included in the FOV of NIRSpec/IFU ( $d_{\text{proj}} < d_{\text{min}}$ ). Interestingly, the small size of the MSA slits has also been found to lead to a possible underestimation of the Ly $\alpha$  flux in Ly $\alpha$  emitters in the presence of a spatial offset between the UV and Ly $\alpha$  emission, or of an extended diffuse Ly $\alpha$  emission (L. Napolitano et al. 2024; M. Nakane et al. 2024).

We find a total number density of Pop III systems in galaxies above  $M_* = 10^{7.5} M_\odot$  of  $\sim 1.0/1.8/2.2 \times 10^{-4} \text{ cMpc}^{-3}$  at

<sup>27</sup> The total number of Pop III particles found in each bin among all the simulated cubes is indicated in the plots, serving as a cautionary note regarding the limited statistics at the highest-stellar-mass bins. More reliable results would necessitate even larger simulated boxes or more simulated volumes.

<sup>28</sup> For reference, the relation between stellar mass and dark matter mass in dustyGadget galaxies is shown in Figure 7 of C. Di Cesare et al. (2023).

$z = 8.1/7.3/6.7$ , respectively. Even when neglecting losses due to geometrical effects, this is much lower than the minimum number density predicted, for example, by A. Vikaeus et al. (2022) to detect at least one Pop III system in a single, blind NIRSpec survey with an area of  $0.0034 \text{ deg}^2$  and a sensitivity of  $1.3 \times 10^{-19} \text{ erg s}^{-1} \text{ cm}^{-2}$ : From their Figure 3, even assuming a high Pop III mass of  $\sim 4.4 \times 10^5 M_\odot$  (orange curve), the required number density is of  $\sim 3.5 \times 10^{-2}/8.9 \times 10^{-3}/1.8 \times 10^{-3} \text{ cMpc}^{-3}$  at the same considered redshift points. This might be an indication that blind spectroscopic surveys are not the most efficient strategy to look for Pop III stars in massive galaxies, and that more care is needed to select promising candidates/environments,<sup>29</sup> although note that these results are strongly model dependent.<sup>30</sup>

### 3.3. Expected Pop III Systems in JWST Surveys

Figure 5 shows the predicted number  $N_{\text{III}}$  of He II-emitting Pop III systems in galaxies of various masses ( $7.5 < \text{Log}(M_*/M_\odot) \leq 9.5$ ) at  $z = 8.1$  that are potentially observable with a single pointing of JWST/NIRSpec in its IFU mode, as a function of effective survey volume  $V_{\text{eff}}$ . We consider the systems that would fall within the FOV in the worst possible projection ( $d_{\text{proj}} = d_{3\text{D}}$ ) with any orientation of the instrument ( $d_{\text{proj}} < d_{\text{min}}$ ; see Section 3.2), hence this should be considered as a lower limit.<sup>31</sup> Specifically, we multiply the values of  $n_{\text{III}}$  from the simulations (first panel of Figure 4, golden dashed line) by the comoving volume of JWST surveys at  $z \simeq 8$ , with  $\Delta z = 1$ :

1. The Next Generation Deep Extragalactic Exploratory Public (NGDEEP) survey (S. L. Finkelstein et al. 2021; N. Pirzkal et al. 2023; M. B. Bagley et al. 2024).
2. The Grism Lens-Amplified Survey from Space (GLASS; T. L. Treu et al. 2017; M. Castellano et al. 2022; T. Treu et al. 2022).<sup>32</sup>
3. The Ultradeep NIRSpec and NIRCAM Observations before the Epoch of Reionization (UNCOVER) survey (R. Bezanson et al. 2022; L. J. Furtak et al. 2023; J. R. Weaver et al. 2024).<sup>33</sup>
4. The Cosmic Evolution Early Release Science Survey (CEERS; S. L. Finkelstein et al. 2017, 2022, 2023).<sup>34</sup>
5. The Public Release IMAGING for Extragalactic Research (PRIMER) survey (J. S. Dunlop et al. 2021).<sup>35</sup>
6. The PANORAMIC survey (C. C. Williams et al. 2021).
7. The Cosmic Evolution Survey (COSMOS-Web; C. M. Casey et al. 2023).<sup>36</sup>

<sup>29</sup> For example, the same authors find that a single typical cluster lens is about 20 times more effective for a spectroscopic detection of Pop IIIs than the considered wide-field surveys. In fact, the smaller survey area ( $\sim 0.082 \text{ arcmin}^2$ ) is compensated by higher probabilities to achieve very high magnifications.

<sup>30</sup> In the fiducial model of A. Vikaeus et al. (2022), they assume a constant star formation rate over a timescale of 10 Myr, with stellar populations formed according to a log-normal IMF in the range  $[1, 500] M_\odot$ , with width  $\sigma = 1$  and a characteristic mass of  $60 M_\odot$ . These assumptions result in a much lower He II luminosity of  $\sim 2.64 \times 10^{40} \text{ erg s}^{-1}$  for a Pop III mass of  $\sim 4.4 \times 10^5 M_\odot$  with respect to Equation (1), which requires a magnification  $\sim 3\text{--}4$  to be observable at the considered sensitivity and redshifts.

<sup>31</sup> Although note that considering an average line of sight as in Figure 4 barely changes the results.

<sup>32</sup> <https://glass.astro.ucla.edu/ers/>

<sup>33</sup> <https://jwst-uncover.github.io/>

<sup>34</sup> <https://ceers.github.io/ceersi-first-images-release>

<sup>35</sup> <https://primer-jwst.github.io/>

<sup>36</sup> <https://cosmos.astro.caltech.edu/>

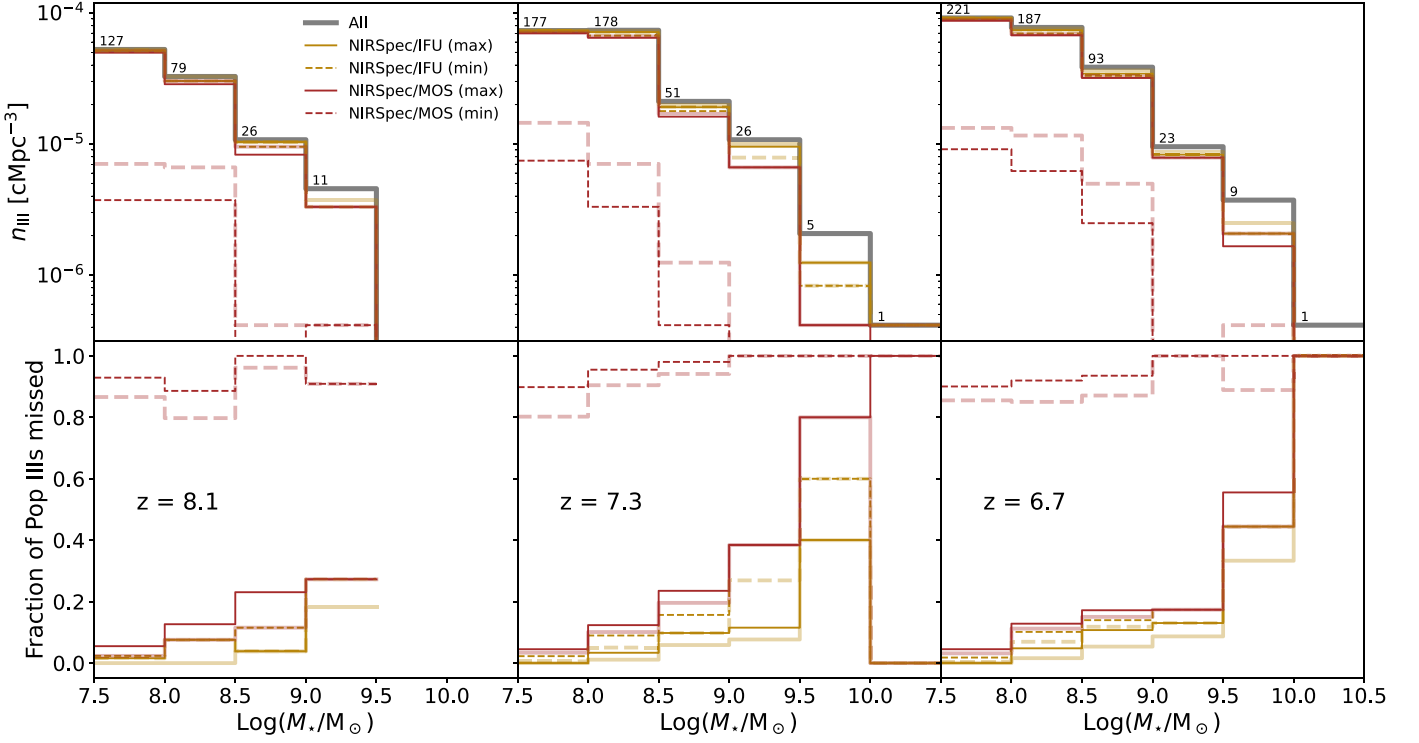


**Figure 4.** Top panels: number density of Pop III particles ( $n_{\text{III}}$ ) that we expect to find at a given redshift  $z$  in halos within a given range of stellar mass  $M_*$  as a function of  $M_*$ , computed in six bins of  $M_*$  (with a spacing of 0.5 dex in the range  $7.5 \leq \text{Log} M_*/M_\odot < 10.5$ ). The total  $n_{\text{III}}$  is shown as a gray solid line, while the  $n_{\text{III}}$  found considering a single pointing of JWST/NIRSpec centered on the host galaxy in the IFU/MOS mode, respectively, are shown as golden/brown lines. The solid/dashed line style refer to the best/worst-case scenario for the orientation for the instrument, considering the worst line of sight to the source and an average line of sight (the latter are shown with thick transparent lines; see text and Figure 3 for details). The total number of Pop III particles found in each bin is also indicated on top of the bins. Bottom panels: fraction of Pop IIIs missed in JWST/NIRSpec pointings, with same color/line style convention. Results are shown for the combined simulated volumes U6, U7, U8, U10, U12, and U13 at redshifts  $z = 8.1$  (left panels),  $z = 7.3$  (middle panels), and  $z = 6.7$  (right panels). We find that a significant number of Pop III systems can be overlooked in these configurations, especially in high-mass galaxies, although this problem appears to be less severe with NIRSpec/IFU thanks to its larger FOV.

Our simulations suggest that more than 400 Pop III systems could be discovered in galaxies with  $M_* \gtrsim 10^{7.5} M_\odot$  around  $z \simeq 8$ , within all these combined JWST fields, and more than one system is supposed to be found within each individual survey. However, we remark that this number is derived from purely geometrical considerations: It indicates the number of Pop III sources—selected from a given survey—that would fall within the NIRSpec FOV when pointing toward the center of their galactic host, while issues related to the intrinsic faintness of the sources and dust absorption/scattering are only broadly discussed in Sections 3.1 and 4.1, respectively. Costly spectroscopic follow-up is in fact required for their identification. Moreover, the number of He II emitters above the sensitivity limits for a given instrumental setup strongly depends on the assumed model for Pop III star formation (see Section 3.1). As an example, only  $\sim 75/85\%$  of the whole range of luminosities spanned by the models in Figure 2 would be covered with a  $\sim 10$  hr exposure at medium spectral resolution, assuming a line width of  $500/50 \text{ km s}^{-1}$ , respectively, while up to  $\sim 90/95\%$  would be covered with a  $\sim 50$  hr exposure.

These Pop III models are likely not equiprobable in reality. Depending on the actual nature of Pop III stars, fainter Pop III models may be favored, causing a large fraction of these systems to only be accessible through very deep exposures; this might be especially true for the more numerous low-mass galaxies, which might be associated with lower star formation efficiencies and hence lower He II luminosities. As discussed in Section 2.2, both the Pop III formation efficiency and IMF

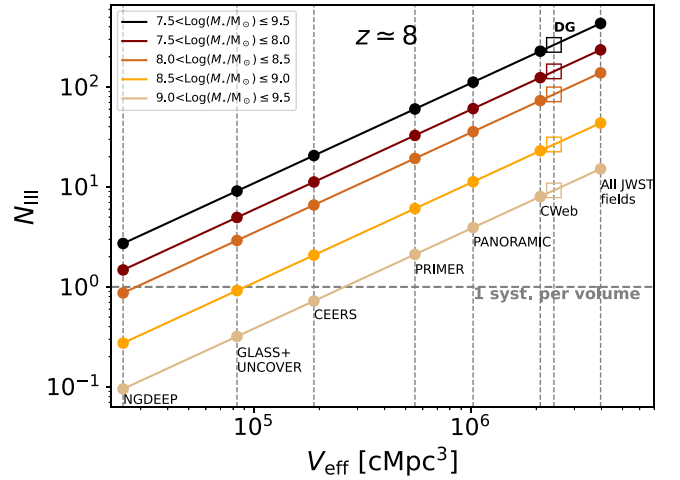


**Figure 5.** Number of potentially observable He II-emitting Pop III systems  $N_{\text{HeII}}$  as a function of the effective survey volume  $V_{\text{eff}}$  at  $z \simeq 8.1$  (see text for details). Vertical dashed lines indicate the effective volume of selected JWST surveys and their cumulative volume at  $z \simeq 8$ , with  $\Delta z = 1$  (filled circles; see text for details); the number of Pop III systems found in our six dustyGadget cubes is also indicated in the plot (DG, empty squares). A horizontal dashed line further indicates the reference value of 1 system per volume. The black line refers to the number found in all halos with  $7.5 < \text{Log}(M_*/M_\odot) \leq 9.5$ , while the colored lines refer to the number found in halos of different stellar mass bins (see Figure 4).

could in fact vary depending on environmental conditions, such as the mass of the dark matter host where the Pop IIIs are formed. We emphasize the need for more in-depth studies of

Pop III star formation in minihalos versus Ly $\alpha$  cooling halos, which would allow us to infer a probability distribution function for the values of the two parameters  $\bar{\epsilon}_{\text{HeII}}$  (Equation (2)) and  $\eta_{\text{III}}$  (Equation (3))—and hence for the He II luminosity  $L_{\text{HeII}}$  (Equation (1))—as a function of host mass.

## 4. Discussion

### 4.1. Dust Absorption/Scattering

In Figure 2, we considered the intrinsic He II emission arising from Pop III star-forming regions. However, light can be removed from our lines of sight to the sources because of both absorption and scattering by interstellar dust, which should be accounted for via an additional factor,  $\sim \exp(-\tau)$  in Equation (1), with  $\tau$  the dust optical depth at  $\lambda = 1640 \text{ \AA}$ . Models of dust mixtures reproducing the observed extinction in the Milky Way (A. Li & B. T. Draine 2001; J. C. Weingartner & B. T. Draine 2001; B. T. Draine 2003a, 2003b, 2003c; M. Glatzle et al. 2019)<sup>37</sup> predict in fact nonnegligible values of the dust absorption cross section per unit dust mass ( $\sim 30\%$  of the peak value) and of the albedo/scattering asymmetry parameter ( $\sim 0.4/0.6$ ) at  $\lambda = 1640 \text{ \AA}$ .<sup>38</sup>

Candidate He II emitters such as GN-z11 (L. Jiang et al. 2021; S. Tacchella et al. 2023), RXJ2129-z8HeII (X. Wang et al. 2024), LAPI (E. Vanzella et al. 2023), and RXCJ2248-ID (M. W. Topping et al. 2024) are consistent with essentially no dust attenuation. However, recent Atacama Large Millimeter/submillimeter Array (ALMA) programs, such as ALPINE and REBELS, have unveiled a population of dusty, obscured star-forming galaxies at  $4 \lesssim z \lesssim 9$ , which is estimated to contribute  $\sim 10\%$ – $25\%$  to the  $z > 6$  cosmic star formation rate density (Y. Fudamoto et al. 2021).<sup>39</sup> The presence of a significant population of red, optically faint galaxies at these redshifts, especially at the high-mass end of the stellar mass function (SMF), is further confirmed by JWST (e.g., M. Xiao et al. 2023; R. Gottumukkala et al. 2024).<sup>40</sup> A lack of prominent emission lines—possibly ascribed to high levels of dust absorption, and/or a combination of low overall star formation rate and intrinsic faintness—has also been reported in the spectra of metal-poor galaxies at  $z \gtrsim 10$  observed with JWST (E. Curtis-Lake et al. 2023; G. Roberts-Borsani et al. 2023).<sup>41</sup>

A detailed estimate of the dampening of the He II line caused by interstellar dust would require full radiative-transfer calculations that are beyond the goals of the present work. However, here we remark that the results shown in Figure 2 should be interpreted as an upper limit, while the actual He II luminosity will depend on the global dust content of the galaxies and on their viewing angle, due to their very

inhomogeneous dust distribution (A. Venditti et al. 2023; see also A. Smith et al. 2019).<sup>42</sup> Focusing on an individual Pop III-hosting galaxy at  $z = 7.3$ , we found that the optical depth ( $\tau$ ) resulting from dust absorption only (i.e., neglecting the contribution of scattering) can vary from  $\sim 10^{-8}$  up to  $\sim 10$ , depending on the specific line of sight to the sources (A. Venditti et al. 2023). Although particularly unfavorable lines of sight might dampen the He II line by up to a factor  $\sim 10^{-9}$  (bringing even the best-case scenario in Figure 2 far below the detectability threshold) we note that the  $\tau$  distribution is peaked around values of order  $\sim 10^{-6}$ – $10^{-1}$ , depending on the position of the considered Pop III stellar population relative to the galactic center (see Table 3 and Figure 12 of A. Venditti et al. 2023). Consequently, typical absorption is much lower, up to a factor  $\sim 0.9$ , i.e., less than 10% of the line flux is absorbed along typical lines of sight. However, we remark that these considerations are based on the study of a single Pop III-hosting galaxy, while a more thorough statistical analysis is required to reliably predict the typical dust absorption in such galaxies; moreover, these estimates do not account for the effect of scattering from dust grains. A strong viewing angle dependence of dust attenuation in high- $z$  galaxies is further demonstrated by R. K. Cochrane et al. (2024). Although their study specifically focused on a sample of massive and obscured HST-dark galaxies at  $4 < z < 7$  rather than Pop III-hosting galaxies, this result further supports the notion that predictions of the extinction based solely on the total dust mass are likely insufficient in high-mass galaxies at these redshifts.

### 4.2. Detecting Pop III through He II versus PISNe

In A. Venditti et al. (2024), we discussed an alternative channel to identify Pop III-hosting galaxies, looking for massive Pop III stars ( $140 M_{\odot} < m < 260 M_{\odot}$ ; A. Heger & S. E. Woosley 2002) at the moment of their death as PISNe. These supernovae are expected to be extremely bright, reaching bolometric luminosities higher than  $\sim 10^{45} \text{ erg s}^{-1}$  during the short shock-breakout phase and  $\sim 10^{44} \text{ erg s}^{-1}$  during their long-term light-curve evolution (D. Kasen et al. 2011), i.e.,  $\sim 2$ – $3$  orders of magnitude brighter than our most optimistic scenario for the He II line. Moreover, they could be more straightforwardly identified even without requiring costly spectroscopic analysis.<sup>43</sup> In fact, the high temperatures required to power He II line emission can be achieved through a number of other confusing mechanisms/sources, including X-ray binaries (D. Schaerer et al. 2019; A. Saxena et al. 2020a, 2020b; P. Senchyna et al. 2020; A. J. Cameron et al. 2024; M. Lecroq et al. 2024), Wolf-Rayet stars (M. Shirazi & J. Brinchmann 2012; C. Kehrig et al. 2018; A. Saxena et al. 2020a; P. Senchyna et al. 2021; F. Martins et al. 2023; G. Tozzi et al. 2023; A. J. Cameron et al. 2024; V. M. A. Gómez-González et al. 2024), active galactic nuclei (M. Shirazi & J. Brinchmann 2012; A. Saxena et al. 2020a, 2020b; G. Tozzi et al. 2023; M. W. Topping et al. 2024; W. Liu et al. 2024), shocks

<sup>37</sup> <https://www.astro.princeton.edu/~draine/dust/dust.html>

<sup>38</sup> A maximum dust absorption cross section per unit dust mass of  $\simeq 1.5 \times 10^3 \text{ cm}^2 \text{ g}^{-1}$  is found assuming an extinction ratio  $R_V = 3.1$  (see, e.g., Figure 1 of M. Glatzle et al. 2019).

<sup>39</sup> Reionization Era Bright Emission Line Survey (R. J. Bouwens et al. 2022).

<sup>40</sup> R. Gottumukkala et al. (2024) find that the obscured galaxy SMF at  $6 < z < 8$  overtakes the pre-JWST SMF around  $\log(M_*/M_{\odot}) \sim 10.375$ . By integrating the SMF at  $\log(M_*/M_{\odot}) > 9.25$ , they estimate that the stellar mass density might even double with respect to pre-JWST studies.

<sup>41</sup> In particular, E. Curtis-Lake et al. (2023) reported  $2\sigma$  upper limits of  $\simeq 6$ – $15.4 \text{ \AA}$  on the He II equivalent widths. Two out of the four analyzed objects also indicate moderate levels of dust (V-band optical depth,  $\tau_V \sim 0.2$ ), albeit with large uncertainties. However, the study of F. D'Eugenio et al. (2023) demonstrates that deep observations can reveal faint lines that were undetected in shallower spectra, as is the case for GS-z12, one of the galaxies previously analyzed in E. Curtis-Lake et al. (2023).

<sup>42</sup> See, e.g., C. Di Cesare et al. (2023) for the dust-to-stellar mass scaling relations of dustyGadget galaxies.

<sup>43</sup> For example, T. Hartwig et al. (2018) and T. J. Moriya et al. (2022) discuss the optimal filter combinations to detect PISNe at  $z \gtrsim 6$  with JWST and with the Nancy Grace Roman Space Telescope, and to discriminate between different types of supernovae (see also F. Y. Wang et al. 2012). In A. Venditti et al. (2024), we further discussed how the peak emission from PISNe can easily outshine the stellar emission of their hosting galaxies, especially in spatially resolved observations.



(C. Kehrig et al. 2018; M. Lecroq et al. 2024), and stellar winds (A. Upadhyaya et al. 2024).

However, the signals from PISNe are very short-lived,  $\sim 1$  yr in the source frame (D. Kasen et al. 2011), compared to  $\sim 1$  Myr for the He II line (D. Schaerer 2002, 2003; H. Katz et al. 2023). The combination of the short lifetime and the limited mass range of PISNe progenitors makes PISNe extremely rare phenomena. In A. Venditti et al. (2024, their Figure 4), we found, at best,  $\sim 0.4$  PISNe on average among galaxies with  $7.5 < \log(M_*/M_\odot) \leq 9.5$  at  $z \simeq 8$ , within the effective volume of all the combined JWST surveys considered in Figure 5, i.e., more than 3 orders of magnitude lower than the predicted number of Pop III He II emitters. Hence, a trade-off between the limitation in statistics for PISNe and the limitation in brightness for the He II signature has to be taken into account when designing our strategies for Pop III detection.

## 5. Conclusions

A systematic search for Pop III stars during the EoR through the He II  $\lambda 1640$  line poses several challenges. We predict more than 400 Pop III systems could be discovered in  $M_* \gtrsim 10^{7.5} M_\odot$  galaxies within existing/ongoing JWST surveys at these redshifts. However, considerable uncertainty surrounds the luminosity of their intrinsic He II emission, which might vary from  $\sim 2 \times 10^{40}$  erg s $^{-2}$  up to  $\sim 10^{42}$  erg s $^{-2}$  depending on the adopted Pop III model. The uncertainty is mainly driven by the assumption on the star formation efficiency parameter  $\eta_{\text{III}}$ , while the presence/absence of mass loss only accounts for a factor of order unity. Different assumptions on the Pop III IMFs can bring these numbers down by up to a factor  $\sim 1/350$ . Dust absorption can also further dampen this emission along unfavorable lines of sight. While promising candidates such as GN-z11 exist (with an inferred high  $\eta_{\text{III}} \sim 0.1$ , and essentially dust-free), it remains unclear how representative such bright targets are. Moreover, many similar targets might fall outside our FOVs, even more than 90% when considering small FOVs as for NIRSpec/MOS.

In principle, a large portion of these Pop III systems could be too faint to be detected in wide—but shallow—blind surveys; for example, the number density  $\sim 1\text{--}2 \times 10^{-4}$  cMpc of our Pop III systems would be too low to yield realistic detection probabilities in the very deep NIRSpec survey considered by A. Vikaeus et al. (2022), when assuming a low He II luminosity of  $\sim 2.64 \times 10^{40}$  erg s $^{-1}$ . A more effective strategy might involve follow-up spectroscopy in the regions surrounding bright, massive galaxies; although rarer, these are in fact more likely to host peripheral Pop III stars (A. Venditti et al. 2023; H. Yajima et al. 2023). Focusing on a limited number of promising targets would truly allow us to push our instrument capabilities, in particular the following:

1. Conducting very deep observations, to confirm/exclude the presence of even the faintest Pop III systems with high confidence (e.g., an exposure of at least 50 hr is required with NIRSpec/IFU at medium resolution to exclude the presence of a  $M_{\text{III}} \gtrsim 2 \times 10^4 M_\odot$  in a galaxy at  $z \sim 6.7$ , assuming a Salpeter-like IMF in the range  $[100, 500] M_\odot$  and strong mass losses; however, the required depth is strongly dependent on the underlying Pop III model).

2. Comprehensively sampling the external regions via multiple pointings, to hunt for Pop III star-forming clumps in the outskirts (ideally, covering a region up to  $\sim 20$  kpc from the galactic center).

In A. Venditti et al. (2023), we found indications that strong accretion of pristine gas from the intergalactic medium at the knots of the cosmic web might favor Pop III star formation. On the other hand, underdense regions with a less progressed history of star formation are also of interest. L. Correa Magnus et al. (2024) suggest a novel formation pathway for Pop IIIs with major mergers as a primary source of gas. However, the role of mergers in the global Pop III star formation budget—and hence whether isolated/interacting galaxies are a better observational target—needs to be confirmed through a more thorough statistical analysis. In future works, we plan to delve into all these aspects, to help us identify the most favorable candidates/environments for follow-up.

## Acknowledgments

We thank Roberto Maiolino for valuable comments. A.V. acknowledges support from Sapienza University of Rome program “Bando mobilità internazionale PhD 2022 (II edizione)” (grant No. 3147/2022, Prot. n. 0102185 del 15/11/2022) during the visiting period (2023 March–September) at UT Austin, Texas (USA). L.G. and R.S. acknowledge support from the PRIN 2022 MUR project 2022CB3PJ3—First Light And Galaxy aSsembly (FLAGS) funded by the European Union—Next Generation EU, and from the Amaldi Research Center funded by the MIUR program “Dipartimento di Eccellenza” (CUP:B81I18001170001).

Part of the JWST data discussed in this article can be obtained from the Mikulski Archive for Space Telescopes (MAST) at the Space Telescope Science Institute. The specific observations can be accessed via C. Cheng (2022) (X. Wang et al. 2024) and M. Rieke et al. (2023) (E. Vanzella et al. 2023).

*Facility:* JWST (NIRSpec).

*Software:* numpy (<https://numpy.org>); S. van der Walt et al. 2011; C. R. Harris et al. 2020), matplotlib (<https://matplotlib.org>); J. D. Hunter 2007), scipy (<https://scipy.org>); P. Virtanen et al. 2020), astropy (<http://www.astropy.org>; Astropy Collaboration et al. 2013, 2018, 2022), JWST Exposure Time Calculator (<https://jwst.etc.stsci.edu>).

## ORCID iDs

Alessandra Venditti  <https://orcid.org/0000-0003-2237-0777>  
 Volker Bromm  <https://orcid.org/0000-0003-0212-2979>  
 Steven L. Finkelstein  <https://orcid.org/0000-0001-8519-1130>  
 Antonello Calabrò  <https://orcid.org/0000-0003-2536-1614>  
 Lorenzo Napolitano  <https://orcid.org/0000-0002-8951-4408>  
 Luca Graziani  <https://orcid.org/0000-0002-9231-1505>  
 Raffaella Schneider  <https://orcid.org/0000-0001-9317-2888>

## References

- Abel, T., Bryan, G. L., & Norman, M. L. 2002, *Sci*, 295, 93  
 Agarwal, B., Johnson, J. L., Zackrisson, E., et al. 2016, *MNRAS*, 460, 4003  
 Aguado, D. S., Caffau, E., Molaro, P., et al. 2023, *A&A*, 669, L4  
 Anders, E., & Grevesse, N. 1989, *GeCoA*, 53, 197  
 Astropy Collaboration, Price-Whelan, A. M., Lim, P. L., et al. 2022, *ApJ*, 935, 167  
 Astropy Collaboration, Price-Whelan, A. M., Sipőcz, B. M., et al. 2018, *AJ*, 156, 123

- Astropy Collaboration, Robitaille, T. P., Tollerud, E. J., et al. 2013, *A&A*, **558**, A33
- Bagley, M. B., Pirzkal, N., Finkelstein, S. L., et al. 2024, *ApJL*, **965**, L6
- Béthermin, M., Fudamoto, Y., Ginolfi, M., et al. 2020, *A&A*, **643**, A2
- Bezanson, R., Labbe, I., Whitaker, K. E., et al. 2022, arXiv:2212.04026
- Bouwens, R. J., Smit, R., Schouws, S., et al. 2022, *ApJ*, **931**, 160
- Bowler, R. A. A., McLure, R. J., Dunlop, J. S., et al. 2017, *MNRAS*, **469**, 448
- Bromm, V. 2013, *RPPH*, **76**, 112901
- Bromm, V., Coppi, P. S., & Larson, R. B. 2002, *ApJ*, **564**, 23
- Bromm, V., Ferrara, A., Coppi, P. S., & Larson, R. B. 2001a, *MNRAS*, **328**, 969
- Bromm, V., Kudritzki, R. P., & Loeb, A. 2001b, *ApJ*, **552**, 464
- Bromm, V., Yoshida, N., Hernquist, L., & McKee, C. F. 2009, *Natur*, **459**, 49
- Cameron, A. J., Katz, H., Witten, C., et al. 2024, *MNRAS*
- Carrasco, E. R., Conselice, C. J., & Trujillo, I. 2010, *MNRAS*, **405**, 2253
- Casey, C. M., Kartaltepe, J. S., Drakos, N. E., et al. 2023, *ApJ*, **954**, 31
- Castellano, M., Fontana, A., Treu, T., et al. 2022, *ApJL*, **938**, L15
- Cheng, C. 2022, RXJ2129 NIRCcam images, STScI/MAST
- Chon, S., Hosokawa, T., Omukai, K., & Schneider, R. 2024, *MNRAS*, **530**, 2453
- Cleri, N. J., Olivier, G. M., Hutchison, T. A., et al. 2023, *ApJ*, **953**, 10
- Cochrane, R. K., Anglés-Alcázar, D., Cullen, F., & Hayward, C. C. 2024, *ApJ*, **961**, 37
- Correa Magnus, L., Smith, B. D., Khochfar, S., et al. 2024, *MNRAS*, **527**, 307
- Curtis-Lake, E., Carniani, S., Cameron, A., et al. 2023, *NatAs*, **7**, 622
- de Bannassuti, M., Salvadori, S., Schneider, R., Valiante, R., & Omukai, K. 2017, *MNRAS*, **465**, 926
- de Bannassuti, M., Schneider, R., Valiante, R., & Salvadori, S. 2014, *MNRAS*, **445**, 3039
- D'Eugenio, F., Maiolino, R., Carniani, S., et al. 2023, arXiv:2311.09908
- Di Cesare, C., Ginolfi, M., Graziani, L., et al. 2024, arXiv:2401.03020
- Di Cesare, C., Graziani, L., Schneider, R., et al. 2023, *MNRAS*, **519**, 4632
- Draine, B. T. 2003a, *ARA&A*, **41**, 241
- Draine, B. T. 2003b, *ApJ*, **598**, 1017
- Draine, B. T. 2003c, *ApJ*, **598**, 1026
- Dunlop, J. S., Abraham, R. G., Ashby, M. L. N., et al. 2021, PRIMER: Public Release IMaging for Extragalactic Research, JWST Proposal. Cycle 1, ID. # 1837
- Faisst, A. L., Schaerer, D., Lemaux, B. C., et al. 2020, *ApJS*, **247**, 61
- Finkelstein, S. L., Dickinson, M., Ferguson, H. C., et al. 2017, The Cosmic Evolution Early Release Science (CEERS) Survey, JWST Proposal ID 1345. Cycle 0 Early Release Science
- Finkelstein, S. L., Papovich, C., Pirzkal, N., et al. 2021, The Next Generation Deep Extragalactic Exploratory Public (NGDEEP) Survey: Feedback in Low-Mass Galaxies from Cosmic Dawn to Dusk, JWST Proposal. Cycle 1, ID. # 2079
- Finkelstein, S. L., Bagley, M. B., Arrabal Haro, P., et al. 2022, *ApJL*, **940**, L55
- Finkelstein, S. L., Bagley, M. B., Ferguson, H. C., et al. 2023, *ApJL*, **946**, L13
- Fraser, M., Casey, A. R., Gilmore, G., Heger, A., & Chan, C. 2017, *MNRAS*, **468**, 418
- Fudamoto, Y., Oesch, P. A., Schouws, S., et al. 2021, *Natur*, **597**, 489
- Furtak, L. J., Zitrin, A., Weaver, J. R., et al. 2023, *MNRAS*, **523**, 4568
- Glatzle, M., Ciardi, B., & Graziani, L. 2019, *MNRAS*, **482**, 321
- Gómez-González, V. M. A., Mayya, Y. D., Zaragoza-Cardiel, J., et al. 2024, *MNRAS*, **529**, 4369
- Gottumukkala, R., Barrufet, L., Oesch, P. A., et al. 2024, *MNRAS*, **530**, 966
- Graziani, L., Schneider, R., Ginolfi, M., et al. 2020, *MNRAS*, **494**, 1071
- Greif, T. H., & Bromm, V. 2006, *MNRAS*, **373**, 128
- Greif, T. H., Johnson, J. L., Klessen, R. S., & Bromm, V. 2008, *MNRAS*, **387**, 1021
- Haardt, F., & Madau, P. 1996, *ApJ*, **461**, 20
- Harris, C. R., Millman, K. J., van der Walt, S. J., et al. 2020, *Natur*, **585**, 357
- Hartwig, T., Bromm, V., Klessen, R. S., & Glover, S. C. O. 2015, *MNRAS*, **447**, 3892
- Hartwig, T., Yoshida, N., Magg, M., et al. 2018, *MNRAS*, **478**, 1795
- Heger, A., & Woosley, S. E. 2002, *ApJ*, **567**, 532
- Hirano, S., Hosokawa, T., Yoshida, N., Omukai, K., & Yorke, H. W. 2015a, *MNRAS*, **448**, 568
- Hirano, S., Hosokawa, T., Yoshida, N., et al. 2014, *ApJ*, **781**, 60
- Hirano, S., Zhu, N., Yoshida, N., Spergel, D., & Yorke, H. W. 2015b, *ApJ*, **814**, 18
- Hosokawa, T., Hirano, S., Kuiper, R., et al. 2016, *ApJ*, **824**, 119
- Hosokawa, T., Omukai, K., Yoshida, N., & Yorke, H. W. 2011, *Sci*, **334**, 1250
- Hunter, J. D. 2007, *CSE*, **9**, 90
- Inoue, A. K. 2011, *MNRAS*, **415**, 2920
- Ishigaki, M. N., Tominaga, N., Kobayashi, C., & Nomoto, K. 2014, *ApJL*, **792**, L32
- Iwamoto, N., Umeda, H., Tominaga, N., Nomoto, K., & Maeda, K. 2005, *Sci*, **309**, 451
- Jaacks, J., Finkelstein, S. L., & Bromm, V. 2019, *MNRAS*, **488**, 2202
- Jakobsen, P., Ferruit, P., Alves de Oliveira, C., et al. 2022, *A&A*, **661**, A80
- Jiang, L., Kashikawa, N., Wang, S., et al. 2021, *NatAs*, **5**, 256
- Kasen, D., Woosley, S. E., & Heger, A. 2011, *ApJ*, **734**, 102
- Katz, H., Kimm, T., Ellis, R. S., Devriendt, J., & Slyz, A. 2023, *MNRAS*, **524**, 351
- Kehrig, C., Vílchez, J. M., Guerrero, M. A., et al. 2018, *MNRAS*, **480**, 1081
- Keller, S. R., Bessell, M. S., Frebel, A., et al. 2014, *Natur*, **506**, 463
- Klessen, R. S., & Glover, S. C. O. 2023, *ARA&A*, **61**, 65
- Latif, M. A., Whalen, D., & Khochfar, S. 2022, *ApJ*, **925**, 28
- Le Fèvre, O., Béthermin, M., Faisst, A., et al. 2020, *A&A*, **643**, A1
- Lecroq, M., Charlot, S., Bressan, A., et al. 2024, *MNRAS*, **527**, 9480
- Li, A., & Draine, B. T. 2001, *ApJ*, **554**, 778
- Liu, B., & Bromm, V. 2020, *MNRAS*, **497**, 2839
- Liu, B., Sibony, Y., Meynet, G., & Bromm, V. 2021, *MNRAS*, **506**, 5247
- Liu, W., Veilleux, S., Canalizo, G., et al. 2024, *ApJ*, **965**, 152
- Magg, M., Schauer, A. T. P., Klessen, R. S., et al. 2022, *ApJ*, **929**, 119
- Maio, U., Ciardi, B., Dolag, K., Tornatore, L., & Khochfar, S. 2010, *MNRAS*, **407**, 1003
- Maio, U., Dolag, K., Ciardi, B., & Tornatore, L. 2007, *MNRAS*, **379**, 963
- Maio, U., Khochfar, S., Johnson, J. L., & Ciardi, B. 2011, *MNRAS*, **414**, 1145
- Maiolino, R., Übler, H., Perna, M., et al. 2024, *A&A*, **687**, A67
- Martins, F., Schaerer, D., Marques-Chaves, R., & Upadhyaya, A. 2023, *A&A*, **678**, A159
- Mas-Ribas, L., Dijkstra, M., & Forero-Romero, J. E. 2016, *ApJ*, **833**, 65
- Matthee, J., Sobral, D., Boone, F., et al. 2017, *ApJ*, **851**, 145
- Moriya, T. J., Quimby, R. M., & Robertson, B. E. 2022, *ApJ*, **925**, 211
- Nakajima, K., & Maiolino, R. 2022, *MNRAS*, **513**, 5134
- Nakane, M., Ouchi, M., Nakajima, K., et al. 2024, *ApJ*, **967**, 28
- Napolitano, L., Pentericci, L., Santini, P., et al. 2024, arXiv:2402.11220
- Pallottini, A., Ferrara, A., Pacucci, F., et al. 2015, *MNRAS*, **453**, 2465
- Pirzkal, N., Finkelstein, S., Papovich, C., & Ngdeep Team 2023, AAS Meeting Abstracts, **55**, 455.04
- Planck Collaboration, Ade, P. A. R., Aghanim, N., et al. 2016, *A&A*, **594**, A13
- Raiter, A., Schaerer, D., & Fosbury, R. A. E. 2010, *A&A*, **523**, A64
- Rauscher, B. J., Arendt, R. G., Fixsen, D. J., et al. 2012, *Proc. SPIE*, **8453**, 84531F
- Rieke, M., Robertson, B., Tacchella, S., et al. 2023, Data from the JWST Advanced Deep Extragalactic Survey (JADES), STScI/MAST
- Rigby, J. R., Lightsey, P. A., García Marín, M., et al. 2023, *PASP*, **135**, 048002
- Roberts-Borsani, G., Treu, T., Chen, W., et al. 2023, *Natur*, **618**, 480
- Rossi, M., Salvadori, S., & Skúladóttir, Á. 2021, *MNRAS*, **503**, 6026
- Rydberg, C.-E., Zackrisson, E., Lundqvist, P., & Scott, P. 2013, *MNRAS*, **429**, 3658
- Salpeter, E. E. 1955, *ApJ*, **121**, 161
- Sarmiento, R., & Scannapieco, E. 2022, *ApJ*, **935**, 174
- Sarmiento, R., Scannapieco, E., & Cohen, S. 2018, *ApJ*, **854**, 75
- Sarmiento, R., Scannapieco, E., & Pan, L. 2017, *ApJ*, **834**, 23
- Sarmiento, R. J., Scannapieco, E., & Pan, L. 2016, AAS Meeting Abstracts, **228**, 319.11
- Saxena, A., Pentericci, L., Mirabelli, M., et al. 2020a, *A&A*, **636**, A47
- Saxena, A., Pentericci, L., Schaerer, D., et al. 2020b, *MNRAS*, **496**, 3796
- Schaerer, D. 2002, *A&A*, **382**, 28
- Schaerer, D. 2003, *A&A*, **397**, 527
- Schaerer, D., Fragos, T., & Izotov, Y. I. 2019, *A&A*, **622**, L10
- Senchyna, P., Stark, D. P., Charlot, S., et al. 2021, *MNRAS*, **503**, 6112
- Senchyna, P., Stark, D. P., Mirocha, J., et al. 2020, *MNRAS*, **494**, 941
- Shirazi, M., & Brinchmann, J. 2012, *MNRAS*, **421**, 1043
- Skinner, D., & Wise, J. H. 2020, *MNRAS*, **492**, 4386
- Smith, A., Ma, X., Bromm, V., et al. 2019, *MNRAS*, **484**, 39
- Sobral, D., Matthee, J., Darvish, B., et al. 2015, *ApJ*, **808**, 139
- Springel, V. 2005, *MNRAS*, **364**, 1105
- Springel, V., & Hernquist, L. 2003, *MNRAS*, **339**, 289
- Stacy, A., Bromm, V., & Lee, A. T. 2016, *MNRAS*, **462**, 1307
- Sugimura, K., Matsumoto, T., Hosokawa, T., Hirano, S., & Omukai, K. 2020, *ApJL*, **892**, L14
- Susa, H., Hasegawa, K., & Tominaga, N. 2014, *ApJ*, **792**, 32
- Tacchella, S., Eisenstein, D. J., Hainline, K., et al. 2023, *ApJ*, **952**, 74
- Thielemann, F. K., Argast, D., Brachwitz, F., et al. 2003, *NuPhA*, **718**, 139
- Topping, M. W., Stark, D. P., Senchyna, P., et al. 2024, *MNRAS*, **529**, 3301
- Tornatore, L., Borgani, S., Dolag, K., & Matteucci, F. 2007a, *MNRAS*, **382**, 1050

- Tornatore, L., Borgani, S., Viel, M., & Springel, V. 2010, *MNRAS*, **402**, 1911
- Tornatore, L., Ferrara, A., & Schneider, R. 2007b, *MNRAS*, **382**, 945
- Tozzi, G., Maiolino, R., Cresci, G., et al. 2023, *MNRAS*, **521**, 1264
- Treu, T., Roberts-Borsani, G., Bradac, M., et al. 2022, *ApJ*, **935**, 110
- Treu, T. L., Abramson, L. E., Bradac, M., et al. 2017, Through the Looking GLASS: A JWST Exploration of Galaxy Formation and Evolution from Cosmic Dawn to Present Day, JWST Proposal ID 1324. Cycle 0 Early Release Science
- Trinca, A., Schneider, R., Valiante, R., et al. 2024, *MNRAS*, **529**, 3563
- Trussler, J. A. A., Conselice, C. J., Adams, N. J., et al. 2023, *MNRAS*, **525**, 5328
- Tumlinson, J., Giroux, M. L., & Shull, J. M. 2001, *ApJL*, **550**, L1
- Tumlinson, J., & Shull, J. M. 2000, *ApJL*, **528**, L65
- Upadhyaya, A., Marques-Chaves, R., Schaerer, D., et al. 2024, *A&A*, **686**, A185
- van den Hoek, L. B., & Groenewegen, M. A. T. 1997, *A&AS*, **123**, 305
- van der Walt, S., Colbert, S. C., & Varoquaux, G. 2011, *CSE*, **13**, 22
- van Dokkum, P. G., Bezanson, R., van der Wel, A., et al. 2014, *ApJ*, **791**, 45
- Vanzella, E., Loiacono, F., Bergamini, P., et al. 2023, *A&A*, **678**, A173
- Venditti, A., Bromm, V., Finkelstein, S. L., Graziani, L., & Schneider, R. 2024, *MNRAS*, **527**, 5102
- Venditti, A., Graziani, L., Schneider, R., et al. 2023, *MNRAS*, **522**, 3809
- Vikaeus, A., Zackrisson, E., Schaerer, D., et al. 2022, *MNRAS*, **512**, 3030
- Virtanen, P., Gommers, R., Oliphant, T. E., et al. 2020, *NatMe*, **17**, 261
- Visbal, E., Bryan, G. L., & Haiman, Z. 2020, *ApJ*, **897**, 95
- Wang, F. Y., Bromm, V., Greif, T. H., et al. 2012, *ApJ*, **760**, 27
- Wang, X., Cheng, C., Ge, J., et al. 2024, *ApJL*, **967**, L42
- Weaver, J. R., Cutler, S. E., Pan, R., et al. 2024, *ApJS*, **270**, 7
- Weingartner, J. C., & Draine, B. T. 2001, *ApJS*, **134**, 263
- Williams, C. C., Oesch, P., Barrufet, L., et al. 2021, PANORAMIC—A Pure Parallel Wide Area Legacy Imaging Survey at 1-5 Micron, JWST Proposal. Cycle 1, ID. # 2514
- Windhorst, R. A., Timmes, F. X., Wyithe, J. S. B., et al. 2018, *ApJS*, **234**, 41
- Woosley, S. E., & Weaver, T. A. 1995, *ApJS*, **101**, 181
- Xiao, M., Oesch, P., Elbaz, D., et al. 2023, arXiv:2309.02492
- Xu, H., Norman, M. L., O'Shea, B. W., & Wise, J. H. 2016, *ApJ*, **823**, 140
- Yajima, H., Abe, M., Fukushima, H., et al. 2023, *MNRAS*, **525**, 4832
- Zackrisson, E., Gonzalez, J., Eriksson, S., et al. 2015, *MNRAS*, **449**, 3057
- Zackrisson, E., Rydberg, C.-E., Schaerer, D., Östlin, G., & Tuli, M. 2011, *ApJ*, **740**, 13
- Zackrisson, E., Zitrin, A., Trenti, M., et al. 2012, *MNRAS*, **427**, 2212